Research Article

Nano Research
2022, 15(6): 5316–5321

ISSN 1998-0124 CN 11-5974/O4
https://doi.org/10.1007/s12274-021-4058-8

Simultaneous switching of supramolecular chirality and organizational chirality driven by Coulomb expansion

Ming-Xia Shi[1], Jiyu Xu[2] (✉), Kai Sun[1], Min-Long Tao[1], Ji-Yong Yang[1], Da-Xiao Yang[1], Zi-Long Wang[1], Zuo Li[1], Jun-Zhong Wang[1] (✉), Qi-Kun Xue[3] (✉), and Sheng Meng[2] (✉)

[1] *School of Physical Science and Technology, Southwest University, Chongqing 400715, China*
[2] *Institute of Physics, Chinese Academy of Sciences, Beijing 100190, China*
[3] *Department of Physics, Tsinghua University, Beijing 100084, China*

Received: 29 September 2021 / **Accepted:** 8 December 2021

ABSTRACT

Chiral switching is a fascinating topic and plays an important role in construction of homochirality. Nevertheless, due to the complexity and flexibility of noncovalent interactions, switching the chirality of entire supramolecular assemblies has hitherto remained a challenge. Here we report the electric field-controlled chirality switching of pentacene pinwheel arrays and two-dimensional (2D) network domains. Pentacene molecules on Cd(0001) surface form the porous network structure with building blocks of hexamer pinwheels. Driven by the electric field from a scanning tunneling microscopy (STM) tip, the supramolecular chirality of pentacene pinwheels and the organizational chirality of entire network domains can be simultaneously switched from one enantiomorph to another. Furthermore, such chiral switching is reversible and repeatable under successive voltage pulses. First-principles calculations demonstrate that electric field significantly modulates the interfacial charge transfer and induces the Coulomb expansion of pentacene layers, and the subsequent reaggregation leads to the chiral flipping of the supramolecular pinwheels and 2D domains. Our results provide a new strategy for dynamic control of the 2D chiral structures and help to steer the supramolecular assembly toward homochirality.

1 Introduction

Chirality is ubiquitous in nature and plays an important role in chemistry, biology, and materials sciences due to the fundamental importance and potential applications [1–7]. Considerable efforts in recent years have been devoted to chiral control by introducing excess enantiomers in chiral amplification [8–11] or external additives in chiral induction [12–17]. As a crucial step of chiral control, chirality switching provides an efficient channel towards formation of extended homochiral domains [18–20]. However, due to the complexity and flexibility of noncovalent interactions, direct flipping the chirality of entire supramolecular assemblies still remains a challenge. Previous studies showed that chiral switching occurs only at the single-molecule level, where the handedness of individual molecules can be reversed by thermal excitation [21] or tunneling electrons [22–25]. Chiral flipping of the supramolecular assemblies in a controlled manner has remained largely unexplored to date.

It remains unclear so far whether the supramolecular assemblies can switch their chirality from one enantiomorph to another. If yes, what kind of external stimulation should be provided to drive such chirality switching? Scanning tunneling microscopy (STM) has proven to be a powerful tool not only to obtain the spatial information at atomic scale, but also to manipulate individual atoms, molecules, or nanostructures on surfaces. Aside from driving the chiral switching of individual molecules, STM tip was also used to initiate chemical reactions and modulate the interfacial adsorption by injecting electrons into the molecular layer [26–29], and provoke structural transitions and trans-cis isomerization by the electric field in tunneling junction [30–37]. Thus one may expect a dramatic effect of the electric field from STM tip on the chiral assemblies and chiral switching.

Not only chiral molecules, but also achiral molecules can form the chiral assemblies when deposited on solid surfaces. Pentacene ($C_{22}H_{14}$) is a typical achiral molecule that consists of five aromatic rings arranged in a linear fashion. It was usually used as a model system to study the molecule-solid interactions in organic semiconductors. On the semimetallic Bi(111) surface, pentacene molecules can form individual large chiral pinwheel clusters with clockwise or anticlockwise handedness [38]. When adsorbed on Ag(111), pentacene molecules were found to form a loosely bound and disordered contact layer at the interface [39, 40]. The divalent hexagonal close-packed metal Cd is usually used as electrode material due to the high redox potential. When deposited on Si(111) substrate, Cd atoms form the crystalline (0001) thin films with the perfectly electronical transparency due to the anisotropic electron motions and quantum-well states [41]. Thus it would be fundamentally important to study the symmetry breaking and molecular assemblies at the pentacene/Cd(0001) interface.

In this work, we reported the simultaneous switching of the supramolecular chirality of pentacene pinwheels and the organizational chirality of entire two-dimensional (2D) domains activated by the electric-field induced Coulomb expansion.

Address correspondence to Jiyu Xu, jiyuxu@iphy.ac.cn; Jun-Zhong Wang, jzwangcn@swu.edu.cn; Qi-Kun Xue, qkxue@mail.tsinghua.edu.cn; Sheng Meng, smeng@iphy.ac.cn

Pentacene molecules on Cd(0001) form the porous network structure with building blocks of hexamer pinwheels. We found that the electric field from STM tip switches the local chirality of pentacene pinwheels and the organizational chirality of 2D network domains, and such chiral switching was reversible and repeatable under successive voltage pulses. First-principles calculations demonstrated that external electric field significantly modulated the interfacial charge transfer and induced the Coulomb expansion of molecular layer, and the subsequent reaggregation leads to the chiral switching of the pentacene pinwheels and 2D domains.

2 Results and discussion

Here we began our experiment by depositing a small amount of pentacene molecules (0.3 monolayer (ML)) on Cd(0001) at room temperature (RT). It was found that the pentacene molecules are highly mobile and cannot be imaged in STM scanning even at 78 K (Fig. 1(a)). The fuzzy noises reflect the nature of 2D molecular gas, resulting from the thermal activated-diffusion. The adsorption of pentacene molecules could induce the absorbate-substrate charge transfer and the interfacial dipole moments (Fig. S1 in the Electronic Supplementary Material (ESM)). Thus, the electrostatic repulsion between pentacene molecules decreased the diffusion barrier of a single pentacene molecule and facilitated the emergence of disordered 2D gas state. The charged molecules occupied the entire substrate terrace homogeneously, similar to the disordered CuPc layers on Ag substrates [42, 43]. Previous studies demonstrated that external electric field can modulate the interfacial adsorption and thus manipulate the interfacial phase transition [31, 35–37]. Therefore, we applied a transient positive voltage pulse to the gaseous adsorbates, which results in condensation and visualization of pentacene molecules. Figure 1(b) shows that the aggregated molecules form a small patch of porous network structure induced by electric field. The emergence of porous structure reflects a delicate interaction between absorbed molecules and underlying substrate.

When pentacene coverage increases to 0.6 ML, large-scale porous network forms spontaneously (Fig. 1(c)). The network phase consists of building blocks of pentacene hexamer pinwheels (three dimers) (Fig. 1(d)), and each pentacene molecule presents two bright spots at the terminals. Nine spots from the six pentacene molecules constitute an anticlockwise (L) pinwheel and achieve a supramolecular chirality. The pentacene hexamers are aligned at the direction deviating 15° from the [$\bar{1}$100] direction of Cd(0001), forming the right (ρ)-enantiomorphous domain (organizational chirality). The lattice constant of pentacene pinwheels is a = 30.5 ± 0.2 Å, corresponding to a high-order-commensurate (HOC) phase ($\sqrt{97} \times \sqrt{97}$) with packing density of 0.74 nm^{-2}. The lattice chirality of ρ-domain can be described as a transformation matrix (11, 3, −3, 8). The porous network phase also includes the clockwise (R) pinwheels, which appeared in the left (λ)-enantiomorphous domains. The transformation matrix of λ-enantiomorphous domain is (8, −3, 3, 11). The ρ- and λ-domains, as well as the L- and R-pinwheels, have a mirror symmetry with respect to the [$\bar{1}$100] direction of Cd(0001) substrate. Overall, the two types of chiral pinwheel domains appear on the entire substrate with equal probabilities based on our statistical analysis (Fig. S2 in the ESM). This network phase can thus be defined as the hexamer pinwheel phase. The pentacene hexamer pinwheels look similar to the reported mixed pinwheels of perylene-3,4,9,10-tetracarboxylic diimide (PTCDI) and 1,3,5-triazine-2,4,6-triamine (melamine) on Au(111) and the chiral pinwheel heterojunctions made of a C_{60} and six pentacene molecules on Cu(111) [44, 45].

We performed first-principles calculations within the framework of density functional theory (DFT) (see Methods for details) to account for formation mechanisms. The optimized structure of L-pinwheel within ρ-domain is shown in Fig. 1(e), and the simulated STM images are shown in Fig. 1(f), which agrees well with the experimental observation. When pentacene coverage is increased to ~ 0.8 ML, two compact structures with herringbone and brick-wall packings have been observed as shown in Fig. S3 in the ESM, where the packing density of pentacene molecules is 0.79 and 0.81 nm^{-2}, respectively. Compared with the herringbone and brick-wall packings, the pinwheel phase has the largest formation energy of −1.827 eV/molecule despite of the smallest adsorption density (Table S1 in the ESM), confirming the intrinsic stability of pinwheel phase under zero electric field.

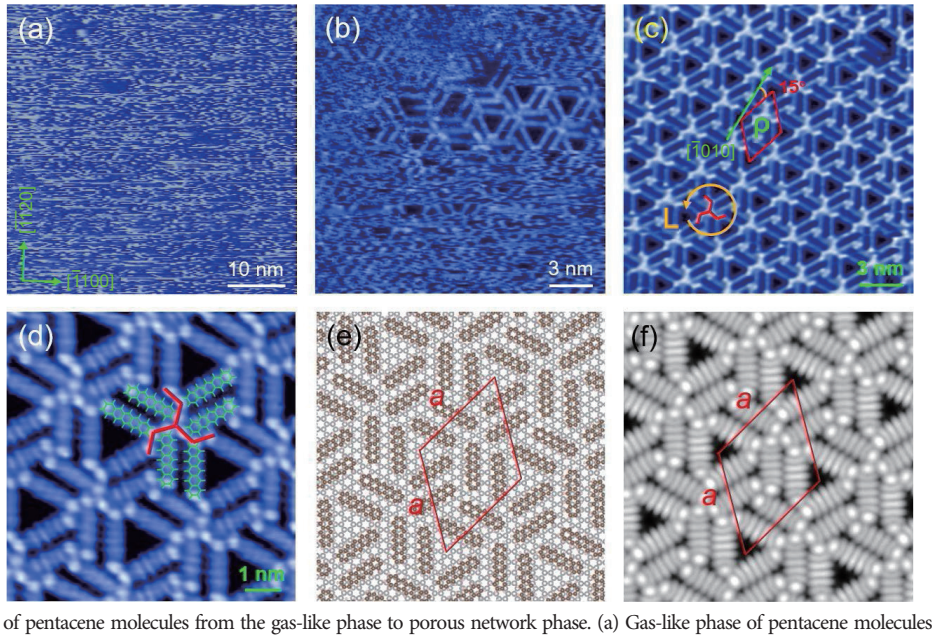

Figure 1 Condensation of pentacene molecules from the gas-like phase to porous network phase. (a) Gas-like phase of pentacene molecules (0.3 ML) on Cd(0001) (0.5 V, 28 pA). (b) A small patch of porous network appears after applying a positive voltage pulse (1.5 V, 21 pA). (c) Large-scale porous network phase with anticlockwise (L-) hexamer pinwheels and ρ-lattices (1.3 V, 21 pA). (d) High-resolution image of the porous network phase (2.3 V, 32 pA). (e) The optimized porous network structure with L-pinwheel and ρ-lattice. (f) The simulated STM image of the network phase with L-pinwheel and ρ-lattices, which is well consistent with experimental image in (d).

Interestingly, by applying a negative voltage pulse, both the supramolecular chirality of pentacene pinwheels and the lattice chirality of 2D pentacene domains can be simultaneously switched from one enantiomorph to another. Figure 2(a) shows a pinwheel phase with ρ-enantiomorphous lattices and L-pinwheels. After a negative voltage pulse (−2.0 V for 50 ms) applied at the cross position, all pinwheels (involving ~ 300 pentacene molecules) switched their chirality from L- to R-enantiomorph. Meanwhile, the lattice chirality is simultaneously switched from ρ- to λ-enantiomorph (Fig. 2(b)). The orientations of pentacene dimers remained unchanged before and after the chiral switching, while the relative alignment in a dimer has now the opposite handed arrangement. The ρ-domains (L-ρ) and the λ-domains (R-λ) were exclusively built up by L-pinwheels and R-pinwheels motifs, respectively. Such combinations between supramolecular chirality and lattice chirality were in contrast with that in chiral pinwheel heterojunctions of C_{60} and pentacene molecules on Cu(111) [45], where the two enantiomorphous pinwheels with opposite handedness co-existed in the same chiral domain. Previously, chiral flipping of 2D domain induced by electric field was observed in the self-assembled networks of CuPc on Cd(0001), where only the organizational chirality was switched from one enantiomorph to another [46].

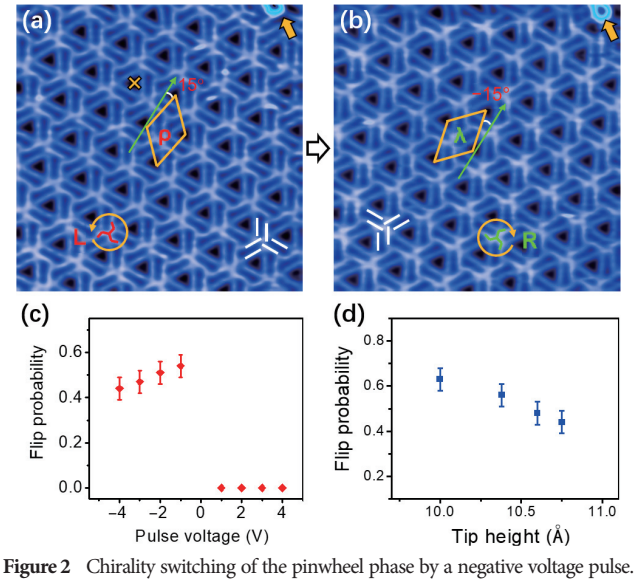

Figure 2 Chirality switching of the pinwheel phase by a negative voltage pulse. (a) A pinwheel domain with ρ-lattice and L-pinwheel before voltage pulse (20 nm × 20 nm, 1.8 V, 22 pA). (b) The obtained λ-lattice and R-pinwheel after voltage pulse of −2 V applied at the cross position in (a). The small island marked by yellow arrow demonstrates the same region is measured. (c) Chiral switching probability versus pulse voltages at a constant tunneling current of 25 pA for 30 ms. Each data point was obtained by repeating the same measurements for 100 times. (d) Chiral switching probability versus tip heights. Each data point was measured by fixing the tip to a specific height and applying a voltage pulse of −2.0 V for 30 ms.

We analyzed statistically the dependence of chiral switching on the pulse conditions. Figure 2(c) shows the variation of chiral switching probability as a function of pulse voltage. It was interesting that the chirality switching occurred only at negative voltages, while no chirality switching was observed under positive voltage pulses. The flipping probability was ~ 50% when the bias voltage changed from 0 to −4 V, indicating the two enantiomorphous domains had the same chance to appear. In addition, the decreasing of tip height obviously increases the chiral switching probability (Fig. 2(d)), while switching probability only shows a weak dependence on tunneling current (Fig. S4 in the ESM). All these results indicated that the observed chirality switching was triggered by the electric field from the STM tip.

To understand the chirality switching processes, we calculated the adsorption of a single pentacene molecule on Cd(0001) under various external electric fields. It is known that the interfacial adsorption could induce the charge transfer and interfacial dipole moment between the flat-lying absorbates and substrates via Pauli repulsion [47–53]. The Bader charge analysis showed that there was ~ 0.5 electron transfer from Cd(0001) substrate to the absorbed pentacene molecule under zero electric field. The charge transfer can be significantly modulated with the external electric field (Fig. 3(c)). A negative electric field of −0.6 V·Å^{-1} increases the charge transfer to 1.1 electron, while a positive electric field of 0.5 V·Å^{-1} leads to the reduction of charge transfer to zero.

Therefore, a negative pulse will drag more electrons from the substrate to pentacene layers and enhance the intermolecular repulsion, thus leading to the lattice expansion of the pentacene layers (Fig. 3(a)). More importantly, the large electron transfer will lead to the Rayleigh instability and the succeeding Coulomb explosion of pentacene layers [53–54]. The injection of electrons to pinwheel pentacene monolayer leads to the expansion and explosion (Fig. 3(d) and Fig. S5(a) in the ESM). This scenario explains well the disintegration of a small domain of pinwheel phase (Fig. S6 in the ESM) and the phase transition from brick-wall to pinwheel phase (Fig. S7 in the ESM) under the negative pulses, as both lead to expansion of pentacene layers. On the contrary, a positive voltage pulse will push the excess electrons back to the substrate reducing the intermolecular repulsion, thus leading to the contraction of pentacene layers as shown in Fig. 3(b). This is consistent with the positive-pulse induced condensation and nucleation of gaseous pentacene molecules displayed in Fig. 1(b), where the stronger attractive van der Waals interactions lead to the gathering and self-assembly of gaseous pentacene molecules into ordered structures. We noted that the Coulomb expansion mechanism proposed here can also explain the switching behaviors at liquid/solid interfaces, where open porous and compact structures were formed at negative and positive bias voltages, respectively [35, 36].

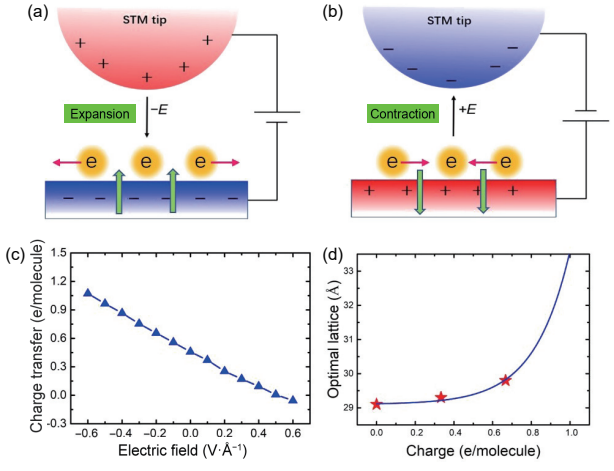

Figure 3 Theoretical calculations of the electric-field-induced chirality switching. (a) and (b) The schematic illustrations for the electric-field induced Coulomb expansion and contraction, respectively. (c) The charge transfer versus the external electric field. The negative value corresponds to the electric fields pointing from the pentacene to substrate. (d) The optimized lattice of the suspended pinwheel phase with various electron injection. The pinwheel phase explodes with electron injection of 1 e/molecule.

Besides the negative voltage pulses, we applied the constant negative scanning voltages to the pentacene pinwheel phases. The pentacene pinwheel phase is always visible at positive bias from 1.0 to 0.2 V, but becomes progressively invisible from −0.6 to −1.8 V due to the instability (Fig. S8 in the ESM). In contrast, the closely-

packed brick-wall phase has not been affected by the variation of voltage, reflecting its relative dynamical stability upon electron injection (Fig. S5 in the ESM). The surrounding brick-wall phase thus constrained the gaseous pentacene molecules. When the bias was switched back to 1.0 V, the pinwheel patterns reappeared. Therefore, the chirality switching of pinwheel phases can thus be interpreted by the Coulomb expansion induced disordering and the subsequent reaggregation of pentacene molecules. The effective range of negative voltage pulses was estimated to be ~ 30 nm. When the size of pinwheel domains was larger than this limit, partial switching may occur. Figure 4(a) shows a big domain with a longitudinal size of 50 nm. After a voltage pulse of –2 V is applied at the flash mark, chirality flipping occurs only at the lower part of the domain, while the upper part of the domain remains unchanged, and a small disordered patch appears between the flipped and un-flipped regions (Fig. 4(b)).

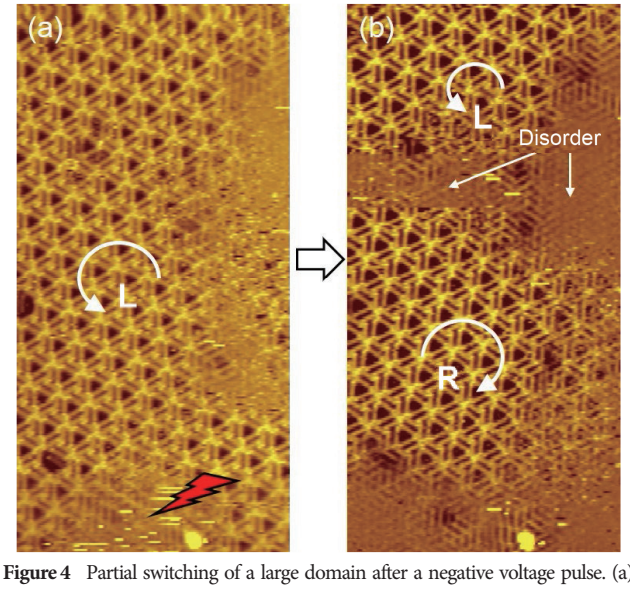

Figure 4 Partial switching of a large domain after a negative voltage pulse. (a) A large domain with L-pinwheel before voltage pulse (25 nm × 50 nm, 1.0 V, 25 pA). (b) Chirality flipping occurs at the lower part of the domain after a voltage pulse of –2 V applied at the flash mark in (a), 25 nm × 50 nm, 1.0 V, 25 pA. The upper part of the domain remains unchanged, and a small disordered patch appears between the flipped and un-flipped regions.

We also found that the chirality switching of pinwheel phases is reversible and repeatable. Two consecutive voltage pulses can lead to two times of chirality switching, i.e., chirality recovery. Shown in Fig. 5(a) is a pinwheel domain with λ-lattice and R-pinwheels. After the first voltage pulse, the chirality switches from R- to L-pinwheels and from λ- to ρ-lattices (Fig. 5(b)). After the second voltage pulse, the chirality is recovered to the original R-pinwheels and λ-lattices (Fig. 5(c)). The repeatability of chiral switching is shown in Fig. (6), where three events of chiral switching occur after applying six voltage pulses. According to our best knowledge, such reversibility and repeatability of chiral switching of supramolecular chirality and lattice chirality have never been reported.

3 Conclusions

In conclusion, the simultaneous switching of supramolecular chirality of pentacene pinwheels and organizational chirality of 2D network domains has been realized by means of electric field induced Coulomb expansion. Distinct from the reported chiral switching events, such chirality switching involves a large number of pentacene molecules within a whole domain. Furthermore, the chiral switching is reversible and repeatable under successive voltage pulses. The electric field controlled chiral switching has several merits. First, it provides a novel and efficient way to realize the large-scale chirality manipulation of self-assembled molecular structures. Second, it offers new insights to manipulate the charged molecules on solid surface by external stimulations. Last, the manipulations of 2D chirality are beneficial to the studies of molecular electronic devices and heterogeneous nucleation and growth.

4 Methods

4.1 STM measurements

The experiments were performed in a low-temperature STM system with base pressure below 1.5×10^{-10} Torr. Cd(0001) thin film was prepared by depositing 10 monolayers of Cd on the Si(111)-7 × 7 surface at RT [41]. The Cd(0001) surface exhibited the hexagonal lattices with the lattice constant of 3.0 ± 0.2 Å. Pentacene molecules were deposited from a homemade tantalum boat onto the Cd(0001) substrate held at RT. All STM images were recorded in constant current mode at liquid nitrogen temperature (78 K) using electrochemically etched polycrystalline tungsten tips. Throughout this study, we defined one monolayer of pentacene with the coverage where the close-packed brick-wall phase covers the entire Cd(0001) surface.

4.2 Methods of first-principles calculations

DFT calculations were performed with the Vienna Ab Initio Simulation Package (VASP) [55]. The projector-augmented wave (PAW) pseudopotentials [56] in conjunction with the Perdew–Burke–Ernzerhof (PBE) [57] exchange-correlation functional was used in all calculations. Van der Waals corrections were considered with the Grimme D3 method [58]. The plane-wave basis set with an energy cutoff of 500 eV was used. The geometry optimizations were performed with the forces on each atom less than 0.02 eV·Å^{-1}. The vacuum region of ~ 15 Å was sufficient to eliminate the artificial periodic interactions.

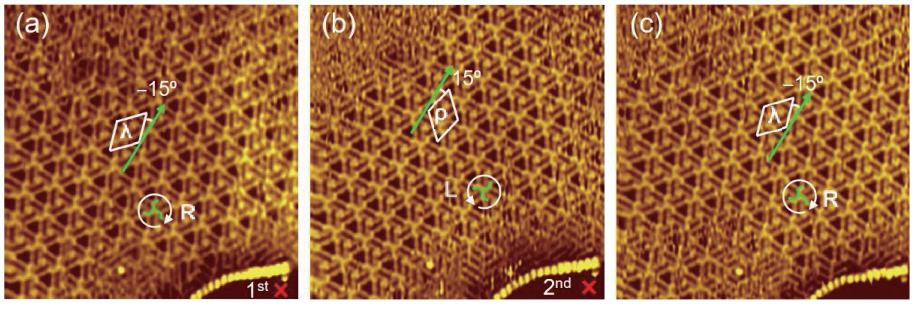

Figure 5 Reversible chiral switching of the pinwheel phases after two successive voltage pulses. (a) A pinwheel domain with λ-enantiomorphous lattice and R-pinwheel before the first voltage pulse. (b) The chirality switches from λ- to ρ-enantiomorphous lattices, and from R- to L-pinwheels after the first voltage pulse. (c) Chirality recovery of the pinwheel domain after the second voltage pulse. The hexamer pinwheels return to the initial λ-lattice and R-pinwheels. All the image sizes are 30 nm × 30 nm, U = 1.4 V, I = 18 pA.

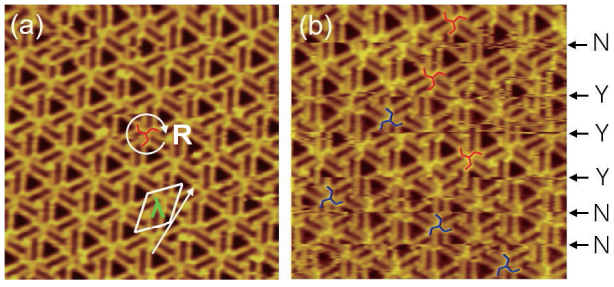

Figure 6 Multiple chiral switching of the pentacene pinwheel phase. (a) A pinwheel domain with λ-enantiomorphous lattice and R-pinwheel before voltage pulses. (b) Six times of voltage pulses lead to three times chiral switching events. The chiral switching and chiral invariance are marked by "Y" and "N", respectively. The image sizes of (a) and (b) are 20 nm × 20 nm, U = 1.6 V, I = 20 pA.

We used the cells of 29.55 Å × 29.55 Å, 25.98 Å × 9.00 Å, and 15.87 Å × 7.94 Å to simulate the pinwheel, herringbone, and brick-wall phases on Cd(0001) substrates, respectively, and the cells used are shown in Fig. 1(e) and Figs. S3(a) and S3(d) in the ESM, respectively. The Brillouin zone was sampled by 1 × 1 × 1, 1 × 3 × 1, and 2 × 3 × 1 Monkhorst–Pack k-mesh for the pinwheel, herringbone, and brick-wall phases, respectively. The single pentacene molecule adsorptions were simulated within a supercell of 24.00 × 24.00 Å, and the Brillouin zone was sampled by 1 × 1 × 1 Monkhorst–Pack k-mesh. Due to the large sizes of various pentacene phases, we chose three layers of Cd atoms and fixed the two bottom layers to simulate the substrates for all adsorption calculations. The external electric field was applied, and the direction of electric field was perpendicular to the slab. The charge transfers were based on the Bader charge calculations.

The total formation energy and the adsorption energy were defined as $E_{formation} = (E_{total} - E_{substrate} - nE_{molecule})/n$ and $E_{adsorption} = (E_{total} - E_{substrate} - E_{molecules})/n$, where E_{total} is the total energy of the pentacene molecules on substrate, $E_{substrate}$ is the energy of the substrate, $E_{molecule}$ is the energy of an isolated pentacene molecule, $E_{molecules}$ is the energy of the pentacene phase, and n is the number of pentacene molecules.

Notes

The authors declare no competing financial interests.

Acknowledgements

This work is supported by the National Natural Science Foundation of China (Nos. 11874304, 11574253, 91850120, and 11934003), Ministry of Science and Technology (No. 2016YFA0300902), and Chinese Academy of Sciences (No. XDB330301).

Electronic Supplementary Material: Supplementary material (differential charge density of pentacene molecule adsorption, experimental and simulated STM images of herringbone and brick-wall phases, phase stabilities of three pentacene phases, formation energies of three pentacene phases) is available in the online version of this article at https://doi.org/10.1007/s12274-021-4058-8.

References

[1] Barlow, S. M.; Raval, R. Complex organic molecules at metal surfaces: Bonding, organization, and chirality. *Surf. Sci. Rep.* **2003**, *50*, 201–341.

[2] Ernst, K. H. Supramolecular surface chirality. In *Supramolecular Chirality*. Crego-Calama, M.; Reinhoudt, D. N., Eds.; Berlin, Heidelberg: Springer, 2006; pp 209–252.

[3] Elemans, J. A. A. W.; De Cat, I.; Xu, H.; De Feyter, S. Two-dimensional chirality at liquid-solid interfaces. *Chem. Soc. Rev.* **2009**, *38*, 722–736.

[4] Lorenzo, M. O.; Baddeley, C. J.; Muryn, C.; Raval, R. Extended surface chirality from supramolecular assemblies of adsorbed chiral molecules. *Nature* **2000**, *404*, 376–379.

[5] Kühnle, A.; Linderoth, T. R.; Hammer, B.; Besenbacher, F. Chiral recognition in dimerization of adsorbed cysteine observed by scanning tunnelling microscopy. *Nature* **2002**, *415*, 891–893.

[6] Haq, S.; Liu, N.; Humblot, V.; Jansen, A. P. J.; Raval, R. Drastic symmetry breaking in supramolecular organization of enantiomerically unbalanced monolayers at surfaces. *Nat. Chem.* **2009**, *1*, 409–414.

[7] Stetsovych, O.; Švec, M.; Vacek, J.; Chocholoušová, J. V.; Jančařík, A.; Rybáček, J.; Kosmider, K.; Stará, I. G.; Jelínek, P.; Starý, I. From helical to planar chirality by on-surface chemistry. *Nat. Chem.* **2017**, *9*, 213–218.

[8] Fasel, R.; Parschau, M.; Ernst, K. H. Amplification of chirality in two-dimensional enantiomorphous lattices. *Nature* **2006**, *439*, 449–452.

[9] Gellman, A. J.; Huang, Y.; Feng, X.; Pushkarev, V. V.; Holsclaw, B.; Mhatre, B. S. Superenantioselective chiral surface explosions. *J. Am. Chem. Soc.* **2013**, *135*, 19208–19214.

[10] Yun, Y. J.; Gellman, A. J. Adsorption-induced auto-amplification of enantiomeric excess on an achiral surface. *Nat. Chem.* **2015**, *7*, 520–525.

[11] Cao, H.; De Feyter, S. Amplification of chirality in surface-confined supramolecular bilayers. *Nat. Commun.* **2018**, *9*, 3416.

[12] Parschau, M.; Romer, S.; Ernst, K. H. Induction of homochirality in achiral enantiomorphous monolayers. *J. Am. Chem. Soc.* **2004**, *126*, 15398–15399.

[13] Masini, F.; Kalashnyk, N.; Knudsen, M. M.; Cramer, J. R.; Laegsgaard, E.; Besenbacher, F.; Gothelf, K. V.; Linderoth, T. R. Chiral induction by seeding surface assemblies of chiral switches. *J. Am. Chem. Soc.* **2011**, *133*, 13910–13913.

[14] Tahara, K.; Yamaga, H.; Ghijsens, E.; Inukai, K.; Adisoejoso, J.; Blunt, M. O.; De Feyter, S.; Tobe, Y. Control and induction of surface-confined homochiral porous molecular networks. *Nat. Chem.* **2011**, *3*, 714–719.

[15] Chen, T.; Yang, W. H.; Wang, D.; Wan, L. J. Globally homochiral assembly of two-dimensional molecular networks triggered by co-absorbers. *Nat. Commun.* **2013**, *4*, 1389.

[16] Nuermaimaiti, A.; Bombis, C.; Knudsen, M. M.; Cramer, J. R.; Laegsgaard, E.; Besenbacher, F.; Gothelf, K. V.; Linderoth, T. R. Chiral induction with chiral conformational switches in the limit of low "sergeants to soldiers" ratio. *ACS Nano* **2014**, *8*, 8074–8081.

[17] Fang, Y.; Ghijsens, E.; Ivasenko, O.; Cao, H.; Noguchi, A.; Mali, K. S.; Tahara, K.; Tobe, Y.; De Feyter, S. Dynamic control over supramolecular handedness by selecting chiral induction pathways at the solution-solid interface. *Nat. Chem.* **2016**, *8*, 711–717.

[18] Berg, A. M.; Patrick, D. L. Preparation of chiral surfaces from achiral molecules by controlled symmetry breaking. *Angew. Chem., Int. Ed.* **2005**, *44*, 1821–1823.

[19] Choi, B. Y.; Kahng, S. J.; Kim, S.; Kim, H.; Kim, H. W.; Song, Y. J.; Ihm, J.; Kuk, Y. Conformational molecular switch of the azobenzene molecule: A scanning tunneling microscopy study. *Phys. Rev. Lett.* **2006**, *96*, 156106.

[20] Li, S. Y.; Chen, T.; Yue, J. Y.; Wang, D.; Wan, L. J. Switching the surface homochiral assembly by surface host-guest chemistry. *Chem. Commun.* **2017**, *53*, 11095–11098.

[21] Weigelt, S.; Busse, C.; Petersen, L.; Rauls, E.; Hammer, B.; Gothelf, K. V.; Besenbacher, F.; Linderoth, T. R. Chiral switching by spontaneous conformational change in adsorbed organic molecules. *Nat. Mater.* **2006**, *5*, 112–117.

[22] Parschau, M.; Passerone, D.; Rieder, K. H.; Hug, H. J.; Ernst, K. H. Switching the chirality of single adsorbate complexes. *Angew. Chem., Int. Ed.* **2009**, *48*, 4065–4068.

[23] Simic-Milosevic, V.; Meyer, J.; Morgenstern, K. Chirality change of chloronitrobenzene on Au(111) induced by inelastic electron tunneling. *Angew. Chem., Int. Ed.* **2009**, *48*, 4061–4064.

[24] Liu, N.; Darling, G. R.; Raval, R. Dynamic chiral flipping within strongly chemisorbed molecular monolayers at surfaces. *Chem. Commun.* **2011**, *47*, 11324–11326.

[25] Bauer, A.; Maier, M.; Schosser, W. M.; Diegel, J.; Paschke, F.; Dedkov, Y.; Pauly, F.; Winter, R. F.; Fonin, M. Tip-induced inversion of the chirality of a molecule's adsorption potential probed by the switching directionality. *Adv. Mater.* **2020**, *32*, 1907390.
[26] Maksymovych, P.; Dougherty, D. B.; Zhu, X. Y.; Yates, J. T. Jr. Nonlocal dissociative chemistry of adsorbed molecules induced by localized electron injection into metal surfaces. *Phys. Rev. Lett.* **2007**, *99*, 016101.
[27] Maksymovych, P.; Sorescu, D. C.; Jordan, K. D.; Yates, J. T. Jr. Collective reactivity of molecular chains self-assembled on a surface. *Science* **2008**, *322*, 1664–1667.
[28] Chen, L.; Li, H.; Wee, A. T. S. Nonlocal chemical reactivity at organic-metal interfaces. *ACS Nano* **2009**, *3*, 3684–3690.
[29] Ladenthin, J. N.; Grill, L.; Gawinkowski, S.; Liu, S. Y.; Waluk, J.; Kumagai, T. Hot carrier-induced tautomerization within a single porphycene molecule on Cu(111). *ACS Nano* **2015**, *9*, 7287–7295.
[30] Li, M.; den Boer, D.; Iavicoli, P.; Adisoejoso, J.; Uji-i, H.; Van der Auweraer, M.; Amabilino, D. B.; Elemans, J. A. A. W.; De Feyter, S. Tip-induced chemical manipulation of metal porphyrins at a liquid/solid interface. *J. Am. Chem. Soc.* **2014**, *136*, 17418–17421.
[31] Zheng, Q. N.; Liu, X. H.; Liu, X. R.; Chen, T.; Yan, H. J.; Zhong, Y. W.; Wang, D.; Wan, L. J. Bilayer molecular assembly at a solid/liquid interface as triggered by a mild electric field. *Angew. Chem., Int. Ed.* **2014**, *53*, 13395–13399.
[32] Borca, B.; Michnowicz, T.; Pétuya, R.; Pristl, M.; Schendel, V.; Pentegov, I.; Kraft, U.; Klauk, H.; Wahl, P.; Gutzler, R. et al. Electric-field-driven direct desulfurization. *ACS Nano* **2017**, *11*, 4703–4709.
[33] Matvija, P.; Rozbořil, F.; Sobotík, P.; Ošťádal, I.; Pieczyrak, B.; Jurczyszyn, L.; Kocán, P. Electric-field-controlled phase transition in a 2D molecular layer. *Sci. Rep.* **2017**, *7*, 7357.
[34] Alemani, M.; Peters, M. V.; Hecht, S.; Rieder, K. H.; Moresco, F.; Grill, L. Electric field-induced isomerization of azobenzene by STM. *J. Am. Chem. Soc.* **2006**, *128*, 14446–14447.
[35] Cometto, F. P.; Kern, K.; Lingenfelder, M. Local conformational switching of supramolecular networks at the solid/liquid interface. *ACS Nano* **2015**, *9*, 5544–5550.
[36] Velpula, G.; Teyssandier, J.; De Feyter, S.; Mali, K. S. Nanoscale control over the mixing behavior of surface-confined bicomponent supramolecular networks using an oriented external electric field. *ACS Nano* **2017**, *11*, 10903–10913.
[37] Cai, Z. F.; Zhan, G. L.; Daukiya, L.; Eyley, S.; Thielemans, W.; Severin, K.; De Feyter, S. Electric-field-mediated reversible transformation between supramolecular networks and covalent organic frameworks. *J. Am. Chem. Soc.* **2019**, *141*, 11404–11408.
[38] Sun, K.; Shao, T. N.; Xie, J. L.; Lan, M.; Yuan, H. K.; Xiong, Z. H.; Wang, J. Z.; Liu, Y.; Xue, Q. K. Chiral pinwheel clusters lacking local point chirality. *Small* **2012**, *8*, 2078–2082.
[39] Eremtchenko, M.; Temirov, R.; Bauer, D.; Schaefer, J. A.; Tautz, F. S. Formation of molecular order on a disordered interface layer: Pentacene/Ag(111). *Phys. Rev. B* **2005**, *72*, 115430.
[40] Smerdon, J. A.; Bode, M.; Guisinger, N. P.; Guest, J. R. Monolayer and bilayer pentacene on Cu(111). *Phys. Rev. B* **2011**, *84*, 165436.
[41] Tao, M. L.; Xiao, H. F.; Sun, K.; Tu, Y. B.; Yuan, H. K.; Xiong, Z. H.; Wang, J. Z.; Xue, Q. K. Visualizing buried silicon atoms at the Cd-Si(111)-7 × 7 interface with localized electrons. *Phys. Rev. B* **2017**, *96*, 125410.
[42] Stadler, C.; Hansen, S.; Kröger, I.; Kumpf, C.; Umbach, E. Tuning intermolecular interaction in long-range-ordered submonolayer organic films. *Nat. Phys.* **2009**, *5*, 153–158.
[43] Antczak, G.; Boom, K.; Morgenstern, K. Revealing the presence of mobile molecules on the surface. *J. Phys. Chem. C* **2017**, *121*, 542–549.
[44] Silly, F.; Shaw, A. Q.; Castell, M. R.; Briggs, G. A. D. A chiral pinwheel supramolecular network driven by the assembly of PTCDI and melamine. *Chem. Commun.* **2008**, *16*, 1907–1909.
[45] Smerdon, J. A.; Rankin, R. B.; Greeley, J. P.; Guisinger, N. P.; Guest, J. R. Chiral "pinwheel" heterojunctions self-assembled from C_{60} and pentacene. *ACS Nano* **2013**, *7*, 3086–3094.
[46] Wang, Y. L.; Sun, K.; Tu, Y. B.; Tao, M. L.; Xie, Z. B.; Yuan, H. K.; Xiong, Z. H.; Wang, J. Z. Chirality switching of the self-assembled CuPc domains induced by electric field. *Phys. Chem. Chem. Phys.* **2018**, *20*, 7125–7131.
[47] Bauert, T.; Zoppi, L.; Koller, G.; Garcia, A.; Baldridge, K. K.; Ernst, K. H. Large induced interface dipole moments without charge transfer: Buckybowls on metal surfaces. *J. Phys. Chem. Lett.* **2011**, *2*, 2805–2809.
[48] Gonella, G.; Dai, H. L.; Rockey, T. J. Tetracene monolayer and multilayer thin films on Ag(111): Substrate-adsorbate charge-transfer bonding and inter-adsorbate interaction. *J. Phys. Chem. C* **2008**, *112*, 4696–4703.
[49] Baby, A.; Gruenewald, M.; Zwick, C.; Otto, F.; Forker, R.; van Straaten, G.; Franke, M.; Stadtmüller, B.; Kumpf, C.; Brivio, G. P. et al. Fully atomistic understanding of the electronic and optical properties of a prototypical doped charge-transfer interface. *ACS Nano* **2017**, *11*, 10495–10508.
[50] Katayama, T.; Mukai, K.; Yoshimoto, S.; Yoshinobu, J. Thermally activated transformation from a charge-transfer state to a rehybridized state of tetrafluoro-tetracyanoquinodimethane on Cu(100). *J. Phys. Chem. Lett.* **2010**, *1*, 2917–2921.
[51] Müller, K.; Seitsonen, A. P.; Brugger, T.; Westover, J.; Greber, T.; Jung, T.; Kara, A. Electronic structure of an organic/metal interface: Pentacene/Cu(110). *J. Phys. Chem. C* **2012**, *116*, 23465–23471.
[52] Yokoyama, T.; Takahashi, T.; Shinozaki, K.; Okamoto, M. Quantitative analysis of long-range interactions between adsorbed dipolar molecules on Cu(111). *Phys. Rev. Lett.* **2007**, *98*, 206102.
[53] Last, I.; Levy, Y.; Jortner, J. Beyond the Rayleigh instability limit for multicharged finite systems: From fission to Coulomb explosion. *Proc. Natl. Acad. Sci. USA* **2002**, *99*, 9107–9112.
[54] Mason, P. E.; Uhlig, F.; Vaněk, V.; Buttersack, T.; Bauerecker, S.; Jungwirth, P. Coulomb explosion during the early stages of the reaction of alkali metals with water. *Nat. Chem.* **2015**, *7*, 250–254.
[55] Kresse, G. Furthmüller, J. Efficient iterative schemes for *ab initio* total-energy calculations using a plane-wave basis set. *Phys. Rev. B* **1996**, *54*, 11169–11186.
[56] Blöchl, P. E. Projector augmented-wave method. *Phys. Rev. B* **1994**, *50*, 17953–17979.
[57] Perdew, J. P.; Burke, K.; Ernzerhof, M. Generalized gradient approximation made simple. *Phys. Rev. Lett.* **1996**, *77*, 3865–3868.
[58] Grimme, S.; Antony, J.; Ehrlich, S.; Krieg, H. A. A consistent and accurate *ab initio* parametrization of density functional dispersion correction (DFT-D) for the 94 elements H-Pu. *J. Chem. Phys.* **2010**, *132*, 154104.